Clays and Clay Minerals, Vol. 53, No. 2, 179–189, 2005.

CATION-SITE PARTITIONING IN Ti-RICH MICAS FROM BLACK HILL (AUSTRALIA): A MULTI-TECHNICAL APPROACH

EMANUELA SCHINGARO[1], FERNANDO SCORDARI[1], ERNESTO MESTO[1], MARIA FRANCA BRIGATTI[2] AND GIUSEPPE PEDRAZZI[3]

[1] Dipartimento Geomineralogico, Universita' di Bari, via E. Orabona 4, I-70125 Bari, Italy
[2] Dipartimento di Scienze della Terra, Universita' di Modena e Reggio Emilia, P.zza S. Eufemia 19, I-41100 Modena, Italy
[3] Dipartimento di Sanita' Pubblica, Sezione di Fisica, Plesso Biotecnologico Integrato via Volturno 39, I-43100 Parma, Italy

Abstract—The crystal chemistry of Ti-rich trioctahedral micas of plutonic origin, cropping out at Black Hill (South Australia) has been investigated by combining electron microprobe analysis, single crystal X-ray diffraction, Mössbauer spectroscopy and X-ray photoelectron spectroscopy. Chemical analyses have shown the samples taken to be quite homogeneous and Ti-rich ($TiO_2 \approx 7$ wt.%). Mössbauer investigation yielded $Fe^{2+}/Fe^{3+} \approx 30$. X-ray photoelectron spectroscopy analysis seems to suggest the occurrence of three Ti species: octahedral Ti^{4+}(60%), octahedral Ti^{3+}(26%), and tetrahedral Ti^{4+}(14%). The analyzed sample belongs to the 1*M* polytype and the relevant crystal data from structure analysis are: $a = 5.347(1)$ Å, $b = 9.261(2)$ Å, $c = 10.195(2)$ Å, $\beta = 100.29°(1)$. Anisotropic structure refinement was performed in space group $C2/m$, and converged at $R = 2.62$, $R_w = 2.80$. Structural details (the *c* cell parameter, the off-center shift of the *M*2 cation towards O4, the bond-length distortions of the *cis*-*M*2 octahedron, the interlayer sheet thickness, the projection of K–O4 distance along *c**, the difference $<K-O>_{outer}-<K-O>_{inner}$) support the occurrence of the Ti-oxy substitution ($^{VI}R^{2+} + 2(OH)^- \rightleftharpoons {}^{VI}Ti^{4+} + 2O^{2-} + H_2$) in the sample. Analysis of structural distortions as a function of the Ti content revealed that the positions of the oxygens O3 and O4 are displaced in opposite senses along [100]. This produces an enlargement of the *M*1 site with respect to the *M*2 site and a shortening of the interlayer distance. This trend seems to be in common with other Ti-rich 1*M* micas of plutonic origin.

Key Words—Crystal Chemistry, Mössbauer Investigation, Structure Refinement, Ti Substitutions, Trioctahedral Micas 1*M*, XPS Investigation.

INTRODUCTION

The micas are a group of minerals occurring in rocks of different origins and form in a wide range of chemical and physical conditions. A deep knowledge of the structural details and of their variations as a function of pressure, temperature, chemistry and other physico-chemical variables of the crystallization environment is important if these mineral phases are to be used as petrogenetic indicators. Ti-bearing micas are of particular interest from this point of view. The connection between crystal chemistry and petrology was recently highlighted in works on metamorphic Ti-rich biotites (Henry and Guidotti, 2002; Cesare *et al*., 2003). Nevertheless, it is generally recognized that it is more difficult to draw petrological implications from biotites of igneous origin, since their compositional variation depends not only on variables such as temperature, oxygen fugacity and bulk composition, but also on the composition of the coexisting melt (Virgo and Popp, 2000; Righter *et al*., 2002).

In addition, the crystal chemistry of these phases has always been quite a challenge because of the large number of cation substitutions which involve tetrahedral (Si, Al, Fe^{3+}), octahedral (Mg, Mn, Fe^{2+}, Fe^{3+}, Ti, Al, Cr), interlayer (K, Ba, Na) and anion (OH^-, O^{2-}, Cl^-, F^-) sites. The mechanisms through which Ti is incorporated into the mica structure are still debated (see Waters and Charnley, 2002 for a review). The most common substitution mechanisms are the following:

(1) $2\ {}^{VI}R^{2+} \rightleftharpoons {}^{VI}Ti^{4+} + {}^{VI}\square$, known as Ti-vacancy (Forbes and Flower, 1974)

(2) $^{VI}R^{2+} + 2\ {}^{VI}Si^{4+} \rightleftharpoons {}^{VI}Ti^{4+} + 2\ {}^{VI}Al^{3+}$, known as Ti-Tschermak (Robert, 1976)

(3) $^{VI}R^{2+} + 2(OH)^- \rightleftharpoons {}^{VI}Ti^{4+} + 2O^{2-} + H_2$, known as Ti-oxy (Bohlen *et al*., 1980) or, as suggested by Dyar *et al*. (1993), a deprotonation mechanism.

Recent investigations have ascertained that Fe-oxy ($^{VI}R^{2+} + (OH)^- \rightleftharpoons {}^{VI}Fe^{3+} + O^{2-} + \frac{1}{2}H_2$) and Ti-oxy substitutions play a major role in phlogopites (Virgo and Popp, 2000; Righter *et al*., 2002; Cesare *et al*., 2003). In all the proposed substitution mechanisms, Ti is assumed to occur in the oxidation state 4+. However, whenever Fe and Ti coexist in a mineral phase, their speciation should be specifically investigated using the most suitable methods. The crystal chemistry of Ti in minerals and, in particular, the occurrence of Ti^{3+} is a widely debated topic (see Malitesta *et al*., 1995; Scordari *et al*., 1999, for a review). The main objection against the occurrence of Ti^{3+} in minerals is that it would imply

* E-mail address of corresponding author:
f.scordari@geomin.uniba.it
DOI: 10.1346/CCMN.2005.0530208

oxygen fugacity values incompatible with the conditions normally occurring on the Earth's crust. However, in a crystal structure, the Ti^{3+} electronic environment might be isolated by rapid crystallization, so that extremely low values of oxygen fugacity would no longer be required to stabilize Ti^{3+} (Waychunas, 1987). In addition, recent studies suggest that the occurrence of cations in unusual oxidation states (*i.e.* Fe^{3+} in trioctahedral micas) and/or of hydrogen in a mineral structure might reflect crystal chemical rather than oxygen fugacity constraints (Righter *et al*., 2002).

Incontrovertible evidence of the presence of Ti^{3+} was not obtained via numerous element-sensitive spectroscopic techniques, such as X-ray absorption near edge spectroscopy, X-ray absorption spectroscopy, electron energy loss spectroscopy (Waychunas, 1987; Otten and Busek, 1987; de Groot *et al*., 1992). Direct evidence of the presence of Ti^{3+} was found in melanitic garnets from Mt. Vulture using X-ray photoelectron spectroscopy (XPS) (Malitesta *et al*., 1995). Very recently Rager *et al*. (2003) have found Ti^{3+} using electron paramagnetic resonance in a single crystal of synthetic pyrope with composition $Mg_{3.01}Al_{1.93}Ti_{0.04}Si_{3.00}O_{12}$, and Nazzareni *et al*. (2004) have been able to synthesize $Ti^{3+,4+}$-bearing diopsides.

In the present work the crystal chemistry of Ti-rich trioctahedral 1*M* mica from late Delamerian potassic gabbronorites cropping out at Black Hills, Australia (Turner, 1996) was investigated via a multi-analytical approach, which combines single crystal X-ray diffraction (SCXRD) techniques, chemical-analytical techniques (electron microprobe analysis (EMPA)), and spectroscopic techniques (Mössbauer spectroscopy and XPS).

The aims of the work are the following: (1) structural characterization of trioctahedral 1*M* micas from Black Hills; (2) determination of transition metal (Fe and Ti) speciation; (3) characterization of the cation ordering; (4) determination of the substitution mechanisms, especially those relevant to Ti.

MATERIALS AND METHODS

The phlogopites under investigation belong to potassic gabbronorite plutons cropping out at Black Hills (south Australia), dated 489±39 Ma on the basis of the Sm-Ne isochrones, and formed following a tholeiitic crystallization path under high temperature (1200−1000ºC), low pressure (~1 kbar), and moderate f_{O_2} (~QFM) conditions (Turner, 1996). Phlogopite in potassic gabbronorites reaches 3−5.5 modal % and is magmatic.

Chemical compositions (Table 1) were measured on polished mineral sections by means of a Cameca SX-50 electron microprobe. Operating conditions were: 15 kV accelerating voltage, 15 nA specimen beam current, and 10 μm beam diameter. The analyses were carried out with wavelength dispersive spectrometers for F, Na, K, Ba, Cl, Ti and with energy dispersive LINK spectrometer for Si, Ca, Al, Mg, Fe. The following standards were employed: jadeite (Na); periclase (Mg); wollastonite (Si and Ca); rutile (Ti); corundum (Al), magnetite (Fe), orthoclase (K), barite (Ba), fluor-phlogopite (F), and sylvite (Cl). Data acquisition followed the procedure suggested by Foley (1989). A conversion from X-ray counts to oxide weight percentages (wt.%) was carried out with the LINK Analytical ZAF 4/FLS data reduction system.

X-ray intensity data collections were performed by means of a SIEMENS-P4-RA single-crystal automated four-circle diffractometer with graphite-monochromated MoKα (0.7107 Å) radiation at room temperature on six different single crystals. Only the results of the best refinement, relevant to the sample labeled BHG1-1, are

Table 1. Average microprobe analyses (wt.%) of Black Hill mica (see text) and atomic proportions (atoms per formula unit, a.p.f.u.). Standard deviations are given in parentheses. Site coordination numbers follow the nomenclature rules given by Rieder *et al*. (1998).

	BHG1-1
SiO_2	35.58(79)
Al_2O_3	13.94(32)
MgO	10.74(36)
FeO_{tot}	18.47(80)
TiO_2	6.80(37)
K_2O	9.39(13)
Na_2O	0.02(2)
BaO	0.02(2)
F	0.04(10)
Cl	0.27(5)
Sum	95.27
FeO	17.91
Fe_2O_3	0.62
Atomic proportions (a.p.f.u.)	
Si	2.81
^{IV}Al	1.19
Sum	4.00
^{VI}Al	0.10
Mg	1.27
Fe^{2+}	1.18
Fe^{3+}	0.04
Ti	0.41
Sum	3
K	0.95
Na	–
Ba	–
Sum	0.95
OH^- calc	1.96
F	0.01
Cl	0.03
Sum	2

https://doi.org/10.1346/CCMN.2005.0530208 Published online by Cambridge University Press

reported in Table 2. No significant differences were detected among refinements of the other five samples. For the single crystal labeled BHG1-1, 2730 reflections were measured out of which 838 are independent. After correction for absorption (ψ scan, North *et al*., 1968) and correction for Lorentz and polarization effects, intensities were reduced to structure factors.

Anisotropic structure refinements were carried out in space group *C*2/*m* using the program CRYSTALS (Watkin, 1992). Starting atomic coordinates were from Brigatti *et al*. (1991). Ionized X-ray scattering curves were employed for non-tetrahedral cations, whereas ionized *vs*. neutral species were used for Si and O (Hawthorne *et al*., 1995). Occupancy at octahedral sites was constrained to 1, whereas interlayer and tetrahedral occupancies could, through restraints (Watkin, 1994), assume values greater or less than 1. This procedure allows, in particular, a better fit to the scattering power at tetrahedral sites, where, due to the small difference between their scattering curves, no least-square refinement of Al *vs*. Si was performed.

Mössbauer spectra were recorded on ~150 mg of small single crystals (average dimension 0.4 mm) dispersed in a cylindrical sample holder, at room temperature in transmission geometry, using a source of ^{57}Co/Rh (1 GBq) and a constant acceleration spectrometer. More detail on the experimental conditions and data analysis are reported elsewhere (Scordari *et al*., 1999).

The XPS measurements consisted of survey scans and narrow scans over the regions O1*s*, Mg2*s*, Al2*p*, Si2*p*, Fe2*p*, Ti2*p* and were performed using a Leybold LHS10 spectrometer equipped with a twin anode source (MgKα/AlKα) on samples prepared as pressed pellets. Details on experimental conditions and data analysis are described in Malitesta *et al*. (1995). The charging effect was corrected by adventitious carbon (C*1s*(B.E.) = 284.8 eV) and differential charging was avoided (Malitesta *et al*., 1995). Peaks were analyzed using a Shirley background subtraction and a Gaussian-Lorentzian curve-fitting algorithm (Desimoni and Malitesta, 1986).

RESULTS AND DISCUSSION

Chemical analyses

Electron microprobe analyses of the same crystal used for structure refinement were unacceptable because of the excessively low oxide total (90%), due to the very small thickness of the crystal. For this reason, and in order to test the homogeneity of the sample, additional analyses were carried out on ten spare crystals which had been mounted in epoxy resin both parallel and perpendicular to the basal planes. These two mounts yielded no significant compositional differences. Accordingly, the average over the whole data set (66 analyses) can be considered as representative of the chemistry of the single crystal used for XRD measurements and is reported in Table 1.

Trioctahedral micas from Black Hill turned out to be quite homogeneous in nature. The worst minimum-maximum ranges found for chemical analyses belonging to the same single crystal were the following: SiO_2 33.65–35.86 wt.%, Al_2O_3 12.83–13.79 wt.%, FeO 18.62–19.47 wt.%, MgO 10.91–11.68 wt.%, TiO_2 6.37–7.25 wt.%, K_2O 9.20–9.61 wt.%, Cl 0.18–0.27 wt.%. Furthermore, the Ti content is one of

Table 2. Crystal data and details of data collection and refinement (see text).

	BHG1-1
Crystal size (mm)	$0.20 \times 0.16 \times 0.01$
Cell setting	Monoclinic
Space group	*C*2/*m*
a,*b*,*c* (Å)	5.347(1), 9.261(2), 10.195(2)
β (°)	100.29(1)
V (Å^3)	496.72(13)
Absorption correction	Empirical
T_{min}/T_{max}	0.65
Number of measured, independent and observed reflections	2730, 838, 692
Criterion for observed reflections	$I > 3\sigma(I)$
R_{int} (%)	3.42
θ_{max}(°)	32
Range of *h*,*k*,*l*	$-8 \leqslant h \leqslant 8$ $-14 \leqslant k \leqslant 14$ $-15 \leqslant l \leqslant 15$
Refinement on	F
R, R_w (%), *S*	2.62, 2.80, 3.12
Number of reflections	692
Number of parameters	68
Weighting scheme	$w = 1$
$\Delta\rho_{min}$,$\Delta\rho_{max}$ (e/Å^3)	−0.35, 1.03

https://doi.org/10.1346/CCMN.2005.0530208 Published online by Cambridge University Press

Table 3. Results of structure refinements in space group *C*2/*m*: crystallographic coordinates, equivalent isotropic (Å^2) and anisotropic displacement parameters of Black Hill mica. Atom labeling from Brigatti *et al.* (1991).

Atom	*x/a*	*y/b*	*z/c*	U_{iso}	U_{11}	U_{22}	U_{33}	U_{12}	U_{13}	U_{23}
K	0	0.5	0	0.034	0.0289(7)	0.0310(8)	0.043(1)	0	0.0050(6)	0
T	0.0742(1)	0.16704(7)	0.22505(7)	0.0087	0.0068(3)	0.0073(3)	0.0135(3)	−0.0003(3)	0.0022(2)	−0.0001(2)
*M*1	0	0	0.5	0.0084	0.0070(4)	0.0059(4)	0.0160(5)	0	0.0039(3)	0
*M*2	0	0.33707(8)	0.5	0.0103	0.0056(3)	0.0129(3)	0.0154(4)	0	0.0017(2)	0
O1	0.0258(6)	0	0.1689(3)	0.0182	0.026(2)	0.012(1)	0.019(2)	0	0.001(1)	0
O2	0.3191(4)	0.2357(2)	0.1674(2)	0.0183	0.016(1)	0.024(1)	0.019(1)	−0.0030(8)	0.0043(7)	−0.0069(7)
O3	0.1312(3)	0.1688(2)	0.3909(2)	0.0111	0.0096(8)	0.0105(9)	0.0145(9)	−0.0004(7)	0.0035(6)	0.0001(6)
O4	0.1280(5)	0.5	0.3967(3)	0.0131	0.009(1)	0.014(1)	0.019(2)	0	0.0033(9)	0

the highest among igneous biotites (see Righter *et al.*, 2002). In Table 1 the total iron (FeO_{tot}) from electron microprobe analyses is partitioned into FeO and Fe_2O_3 based on Mössbauer results (see below). In order to obtain the best crystal chemical formula, microprobe analyses were normalized to seven cations and the Ti deprotonation mechanism was considered. A crystal chemical formula which takes into account the results of XPS investigations is also discussed (see the crystal chemistry sections below).

Structural investigations

Preliminary analyses of Weissenberg photographs revealed that the 1*M* and $2M_1$ polytypes coexist in separate crystals of micas from Black Hill. The single crystal considered in the present work belongs to the former polytype. Its main crystal data are listed in Table 2 whereas the results of an anisotropic structure refinement in space group *C*2/*m* are reported in Tables 3−5 in terms of atomic coordinates and anisotropic displacement factors (Table 3), selected bond

Table 4. Selected parameters derived from the structure refinements in space group *C*2/*m* of Black Hill mica.

BHG1-1			
T−O1 (Å)	1.654(1)	Volume$_T$ (Å^3)	2.331
T−O2 (Å)	1.655(2)	τ (°)	110.28
T−O2′ (Å)	1.653(2)	α (°)	5.72
T−O3 (Å)	1.664(2)	Δz (Å)	0.015
<*T*−O> (Å)	1.657	D.M. (Å)	0.476
*M*1−O4(×2) (Å)	2.078(3)	Volume$_{M1}$ (Å^3)	12.11
*M*1−O3(×4) (Å)	2.110(2)	Ψ_{M1} (°)	59.20
<*M*1−O> (Å)	2.099	BLD$_{M1}$	0.683
		ELD$_{M1}$	5.351
*M*2−O4(×2) (Å)	2.028(2)	Volume$_{M2}$ (Å^3)	11.69
*M*2−O3(×2) (Å)	2.106(2)	Ψ_{M2} (°)	58.76
*M*2−O3′(×2) (Å)	2.085(2)	BLD$_{M2}$	1.456
<*M*2−O> (Å)	2.073	ELD$_{M2}$	4.840
		Shift$_{M2}$ (Å)	0.035
K−O1(×2) (Å)	3.023(3)	Δ_{K-O4} (Å))	0.261
K−O1′(×2) (Å)	3.310(3)	t_{K-O4} (Å)	3.915
K−O2(×4) (Å)	3.282(2)		
K−O2′(×4) (Å)	3.034(2)	t_{tet} (Å)	2.256
<K−O>$_{inner}$ (Å)	3.030	t_{oct} (Å)	2.150
<K−O>$_{outer}$ (Å)	3.291	t_{int} (Å)	3.368
<K−O> (Å)	3.161		

Note: τ tetrahedral flattening angle; α tetrahedral rotation angle (Hazen and Burnham, 1973); Δ*z*: departure from coplanarity of the basal O atoms, calculated as $\Delta z = (z_{o2} - z_{o1})c\sin\beta$ (Güven); D.M.: dimensional misfit between tetrahedral and octahedral sheets defined as D.M. = $[2\sqrt{2}<O-O>_{bas} - 3\sqrt{2}<M-O>]$ (Toraya, 1981); ψ: octahedral flattening angles (Donnay *et al.*, 1964a, 1964b); BLD: bond-length distortions calculated as BLD = $100/n * \Sigma_i\ I(M-O)_i - <M-O>I/<M-O>$ (Renner and Lehmann, 1986); ELD: edge-length distortion defined as ELD = $100/n * \Sigma_i\ I(O-O)_i - <O-O>I/<O-O>$) (Renner and Lehman, 1986); Shift$_{M2}$: off-center shift of the *M*2 cation defined as the distance between the refined position of cation and the geometrical center of the *M*2 site (coordinates: *x/a* = 0.0, *y/b* = 0.8333, *z/c* = 0.5); Δ_{K-O4} = <K−O>$_{outer}$ − <K−O>$_{inner}$; t_{K-O4}: projection of K−O4 distance along *c**; t_{tet}: tetrahedral sheet thickness calculated from *z* coordinates of basal and apical O atoms; t_{oct}: octahedral sheet thickness (Toraya, 1981); t_{int} calculated from the *z* coordinates of basal O atoms.

https://doi.org/10.1346/CCMN.2005.0530208 Published online by Cambridge University Press

distances and distortion parameters (Table 4), and mean atomic numbers (Table 5).

The 1*M* polytype, having sharp reflections both for $k = 3n$ and $k \neq 3n$, turned out to be perfectly ordered. The refinement in space group *C*2/*m* converged to $R = 2.62$, $R_w = 2.80\%$; the highest peak in difference Fourier maps (1.03 $e^-/Å^3$) is at the expected position for the hydrogen atom (not refined) at a distance of 0.83 Å from oxygen O4. The differences between octahedral mean bond distances (<*M*1−O>, <*M*2−O>) point to a meso-octahedral character (Ďurovič, 1981, 1994). The difference of ~1 e^- between mean atomic numbers (m.a.n.$_{M1}$−m.a.n$_{M2}$) (see Tables 4 and 5) seems consistent with this conclusion. From inspection of Table 4, it is of note that the distance *M*2−O4 is remarkably short in comparison to the two *M*2−O distances, as was also found for an oxy-biotite from El Joyazo, Spain (Cesare *et al*., 2003). This result seems to indicate a preferential partitioning of Ti^{4+} atoms over the *M*2 site. In addition, the *c* edge is low due to the shortening of the K−O4 distance (Table 4), and the sample is characterized by high values of *M*2-BLD and of the shift of the *M*2 cation from the geometric center of the octahedron, as well as by low values for Δ_{K-O4} and t_{int} (Table 4). All these observations provide strong evidence for the occurrence of Ti-oxy substitution, as previously found by other authors (Takeda and Ross, 1975; Ohta *et al*., 1982; Cruciani and Zanazzi, 1994; Cesare *et al*., 2003). The remaining structural parameters shown in Table 4 are consistent with those found in the literature for phlogopites with similar composition (Brigatti and Guggenheim, 2002).

Table 5. Octahedral cation distribution, mean atomic numbers (m.a.n., e^-) of cation sites, octahedral and tetrahedral mean distances, as determined by structure refinement (X_{ref}) and chemical analysis (EMPA). See text for details.

Sample	Octahedral cation distribution
BHG1-1	*M*1: $(Mg^{2+}_{0.43}Fe^{2+}_{0.53}Fe^{3+}_{0.04})$
	*M*2:$(Mg^{2+}_{0.42}Fe^{2+}_{0.325}Ti_{0.205}Al_{0.05})$
	*M*1 octahedron
*M*1 $e^-_{X\text{-ref}}$	20.09 (20.17)
*M*1 e^-_{EMPA}	19.98
<*M*1−O>$_{X\text{-ref}}$ (Å)	2.099
<*M*1−O>$_{EMPA}$ (Å)	2.109
	*M*2 octahedron
*M*2 $e^-_{X\text{-ref}}$	19.00 (18.89)
*M*2 e^-_{EMPA}	18.65
<*M*2−O>$_{X\text{-ref}}$ (Å)	2.073
<*M*2−O>$_{EMPA}$ (Å)	2.067
$e^-_{(M1+2M2)X\text{-ref}}$	58.09 (57.95)
$e^-_{(M1+2M2)EMPA}$	57.28
	Interlayer site
$Ke^-_{X\text{-ref}}$	19.00 (19.04)
Ke^-_{EMPA}	18.05
	Tetrahedral site
$Te^-_{X\text{-ref}}$	13.86 (13.88)
Te^-_{EMPA}	13.82
<*T*−O>$_{X\text{-ref}}$	1.656
<*T*−O>$_{EPMA}$	1.659

Spectroscopic investigations

The room-temperature Mössbauer spectrum (see Figure 1) consists of two main asymmetric absorptions centered at about −0.2 and 2.3 mm/s ascribed to octahedral Fe^{2+} and a small shoulder at ~1.0 mm/s ascribed to octahedral Fe^{3+}. There was no clear evidence of tetrahedral Fe^{3+} in the sample. Both Lorentzian lineshapes and quadrupole splitting distributions (QSD) (Rancourt and Ping, 1991; Rancourt, 1994a, 1994b; Rancourt *et al*., 1994) were used to fit experimental spectra. As the Lorentzian fittings were not considered very satisfactory, only QSD results are reported (see Table 6 and Figure 1).

The QSD fittings were performed using two generalized sites, one for Fe^{2+} and the other for Fe^{3+}. The dominant Fe^{2+} QSD was assumed to have three Gaussian components, whereas Fe^{3+} QSD was assumed to have just one Gaussian component. A−/A+ ratios were allowed to vary during fitting (see Table 6) to take into account non-ideal orientation randomness of the sample. The QSD method provided statistically consistent fits (see residuals and χ^2 values in Figure 1 and Table 6, respectively) and yielded the following results: $Fe^{2+} = 96.97$, $Fe^{3+} = 3.03\%$, for the sample from Black Hill.

The XPS spectra were measured on powders obtained from the same samples as used for Mössbauer investigations. A survey scan is shown in Figure 2. All the elements expected from the bulk chemistry of the sample are revealed. The raw narrow spectrum of the Ti2*p* photopeak is reported in Figure 3. The full width at half maximum (FWHM) of the Ti2$p_{3/2}$ component is 2.0 eV,

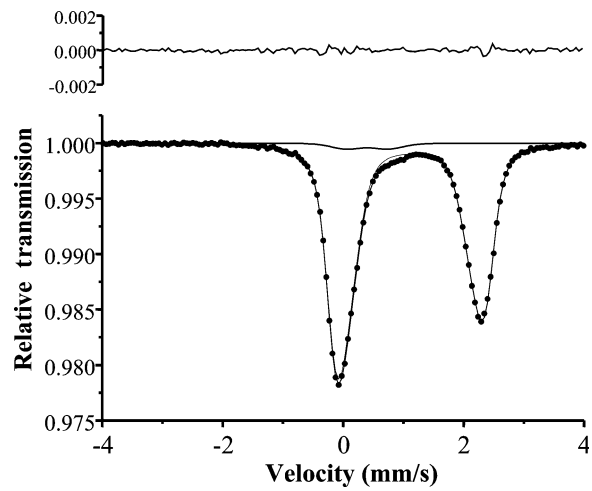

Figure 1. Mössbauer spectrum at room temperature and residuals of sample BHG1-1: fitting according to the QDS method.

https://doi.org/10.1346/CCMN.2005.0530208 Published online by Cambridge University Press

Table 6. Mössbauer parameters obtained by the quadrupole splitting distribution method (see text).

	χ^2	species	Γ/2 (mm/s)	δ_0† (mm/s)	A_-/A_+	ΔE_Q (mm/s)	σ	*P* (%)	*A* (%)
BHG1-1	1.54	Fe^{2+}-1	0.097*	1.1147	1.33	2.09	0.326	48	96.97(68)
		Fe^{2+}-2	0.097*	1.1147	1.33	2.494	0.225	46	
		Fe^{2+}-3	0.097*	1.1147	1.33	1.84	1.51	6	
		Fe^{3+}	0.097*	0.4	1*	0.69	0.43	100*	3.03(68)

†δ_1 = 0 during fitting
*fixed parameter

i.e. too large for a single Ti species to occur in the sample (the expected value of the relevant FWHM being 1.50 eV). The fits to experimental Ti2*p* photopeaks were performed according to a procedure described by Malitesta *et al.* (1995). The best fit is reported in Table 7 and in Figure 4. Three different species of Ti seem to occur in mica under examination: octahedral Ti^{4+} (~60%, B.E. ≈459 eV), tetrahedral Ti^{4+} (~14%, B.E. ≈460 eV), and octahedral Ti^{3+} (~26%, B.E. ≈458 eV). Alternative fittings with only two Ti species (octahedral Ti^{3+} plus octahedral Ti^{4+} and octahedral Ti^{4+} plus tetrahedral Ti^{4+}) provided unacceptable residuals and are not reported. The present results seem to confirm that minor amounts of Ti^{3+} may be found in minerals. As stated in the Introduction, the evidence for the occurrence of Ti^{3+} in crystal structures is rapidly growing (*e.g.* Rager *et al.*, 2003; Nazzareni *et al.*, 2004). It has to be stressed, however, that some potentially suitable techniques for Ti characterization (*i.e.* electron paramagnetic resonance) cannot be used for the micas under investigation because of the coexistence of Fe. For the same reason, previous studies on Ti oxidation states in micas via optical absorption spectroscopy (Schwarcz, 1967; Burns, 1970) cannot be considered conclusive. Indeed, in the case of micas, which have complex structures and compositions, a multi-analytical approach, such as that adopted in this work, is necessary as it permits combination and/or cross-checking of the results (see section below).

Crystal chemistry

Crystal chemical formulae and cation distributions have been obtained by combining electron and spectroscopic data, taking into account the results from structure refinements (mean atomic numbers per site, bond distances, structural effects of cation substitutions, *etc.*).

As a first step, formula recalculation was performed with Dymek's (1983) method without using the Mössbauer data, and yielded:

$$(K_{0.89}\square_{0.11})(Mg_{1.20}Fe^{2+}_{0.58}Fe^{3+}_{0.45}Ti^{4+}_{0.39}\square_{0.39})(Si_{2.66}Al_{1.23}Fe^{3+}_{0.11})O_{10}OH_{1.96}Cl_{0.03}F_{0.01} \quad (1)$$

It can be noted from formula 1 that the Fe^{2+}/Fe^{3+} ratio is inconsistent with Mössbauer data and the calculated mean atomic number, $(M1 + 2M2)_{EMPA}$ = 49.76, is in disagreement with X-ray data (see Table 5). Subsequently, combining EMPA and Mössbauer data, and adopting a model involving seven cations plus Ti-oxy substitution allowed the following crystal chemical formula to be calculated:

$$(K_{0.95}\square_{0.05})(Al_{0.10}Mg_{1.27}Fe^{2+}_{1.18}Fe^{3+}_{0.04}Ti^{4+}_{0.41})(Si_{2.81}Al_{1.19})O_{10.82}OH_{1.14}Cl_{0.03}F_{0.01} \quad (2)$$

In formula 2, Al- and Fe^{3+}-Tschermak mechanisms do not completely balance the excess tetrahedral Al, since 0.10 Al^{3+} a.p.f.u. remain unbalanced.

By introducing our XPS results for Ti oxidation states and partitioning, formula 2 is modified as follows:

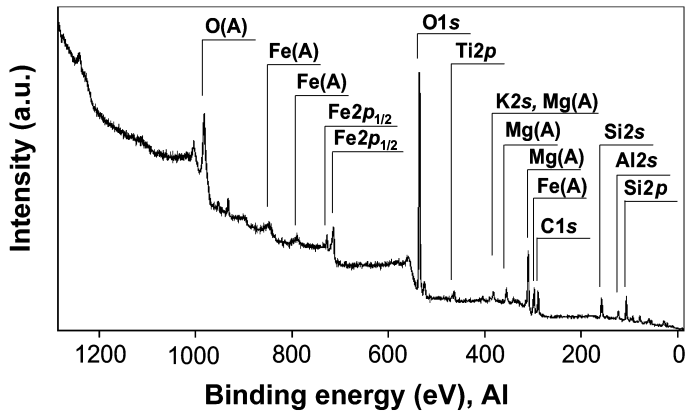

Figure 2. Survey XPS spectrum of sample BHG1-1. Source AlKα. "A" marks Auger signals.

https://doi.org/10.1346/CCMN.2005.0530208 Published online by Cambridge University Press

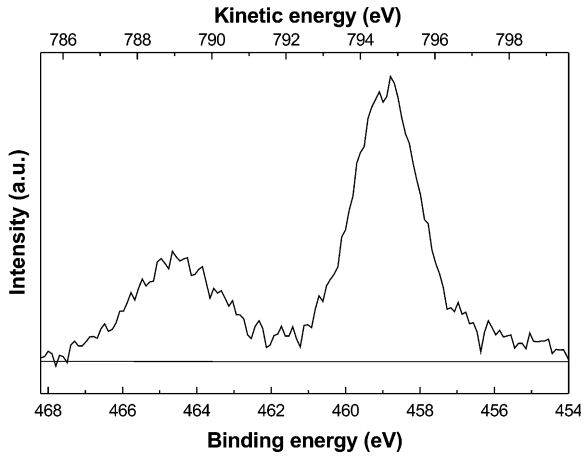

Figure 3. High-resolution raw XPS spectrum for the Ti2*p* region of sample BHG1-1. Source MgKα. The latter source was used to avoid interference on the Ti2*p* region due to the O1*s* satellite peak, always occurring when unmonochromatized AlKα radiation is employed.

$$(K_{0.95}\square_{0.05})(Al_{0.15}Mg_{1.27}Fe^{2+}_{1.18}Fe^{3+}_{0.04}Ti^{4+}_{0.26}Ti^{3+}_{0.10})(Si_{2.81}Al_{1.14}Ti^{4+}_{0.05})O_{10.62}OH_{1.34}Cl_{0.03}F_{0.01} \quad (3)$$

In formulae 2 and 3 the number of OH groups per formula unit have been obtained by charge balancing according to the Ti^{4+}-oxy ($Ti^{4+} + 2O^{2-} + H_2 \rightleftharpoons M^{2+} + 2OH^-$), and Ti^{4+}-oxy and Ti^{3+}-oxy ($^{VI}R^{2+} + (OH)^- \rightleftharpoons {}^{VI}Ti^{3+} + O^{2-} + ½H_2$) substitution schemes, respectively. This choice leads to $0.41 \times 2 = 0.82$ and $0.26 \times 2 + 0.10 = 0.62$ additional oxygen atoms p.f.u. The final OH^- content is, therefore, 1.14 and 1.34 for formulae 2 and 3, respectively. In the present work no direct determination of the H content was carried out. However, Figure 10a in Cesare *et al*. (2003) illustrates the relationship between the *c* cell parameter and the OH content for a number of Ti-rich phlogopites; the H content can be estimated at 1.20–1.30 a.p.f.u., and this is consistent with the values calculated above.

Table 7. Results of XPS investigation of Ti chemical speciation of sample BHG1-1.

	BE (eV)	Species (%)
Ti^{3+}	457.95	26.04 (1.39)
$^{VI}Ti^{4+}$	459.04	60.00 (1.44)
$^{IV}Ti^{4+}$	460.20	13.96 (1.08)

In the final octahedral cation distribution, shown in Table 5, Ti is partitioned into the *M*2 site, whereas Fe^{3+}, as it is not involved in the dehydrogenation process, is partitioned into *M*1 (Cesare *et al*., 2003). This distribution is also supported by an analysis of bond distances and mean atomic numbers. The mean distances <*M*–O> were calculated from EMPA-derived (formula 2 above) molar fractions and both Shannon's radii (Shannon, 1976) and radii tabulated by Weiss *et al*. (1985). Only Shannon's radii provided a good match with those observed from SCXRD data, and of course the agreement is equally good if cation partition is derived from formula 3 above.

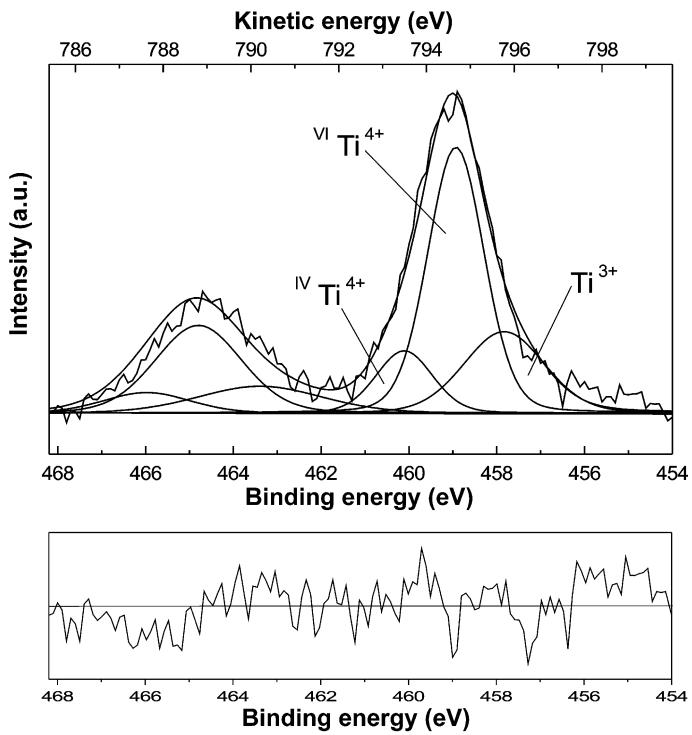

Figure 4. Best fit of the background-subtracted Ti2*p* spectrum of sample BHG1-1. The lower window represents the residual spectrum.

https://doi.org/10.1346/CCMN.2005.0530208 Published online by Cambridge University Press

A good agreement is also found between mean atomic numbers derived from structure refinements (reported in Table 5 with the X-ref subscript) and those calculated from crystal chemical formulae (reported in the table with the EMPA subscript). In addition, in Table 5, the m.a.n. values obtained from structure refinement of sample BHG1-1 are compared with the averaged m.a.n. values (in squared parentheses) from the structure refinements of a further five single crystals (see Materials and Methods). The general agreement confirms the chemical homogeneity of Black Hill micas.

The introduction of tetrahedral Ti^{4+} in formula 3 is in agreement with spectroscopic evidence, such as the absence of tetrahedral Fe^{3+} from Mössbauer spectroscopy, and the occurrence of tetrahedral Ti^{4+} from XPS investigation. However, the occurrence of tetrahedral Ti^{4+} in micas is a matter of debate: Kovalenko *et al.* (1968) claimed they had been able to synthesize micas with tetrahedral Ti, whereas Robert (1976) could not, concluding that only octahedral Ti can be present in micas. Farmer and Boettcher (1981), from optical absorption spectroscopy on phlogopites from kimberlites, suggested the following order of preference for cations in tetrahedral sites: Si > Al > Ti > Fe. On the other hand, much evidence has been found, via different methods, of the occurrence of tetrahedral Fe^{3+} in phlogopites from ultra-alkaline rocks (*e.g.* Ohta *et al.*, 1982; Rancourt *et al.*, 1992; Cruciani *et al.*, 1995; Brigatti *et al.*, 1996). It has already been pointed out above that Ti is not easily studied in minerals, especially in the presence of Fe (see also Waychunas, 1987). As far as tetrahedral Ti^{4+} is concerned, it was unambiguously characterized by a combination of XPS, XANES and EXAFS for Ti-silicalites (Trong On and Bonneviot, 1992), which may contain remarkable amounts of tetrahedral Ti. For the latter species, a B.E.= 459.8 eV was found by these authors. The XPS results obtained in the present work, relevant to the tetrahedral Ti^{4+}, are consistent with those found for Ti-silicalite and with those found in a previous study on natural Ti-garnets (Malitesta *et al.*, 1995).

Layer features in Ti-bearing phlogopites from selected plutonic environments

The structural details of Black Hill mica, which is characterized by unusual Ti content, were compared to analogous information from other plutonic mica samples from the literature. All micas considered were constrained with *C*2/*m* symmetry and they belong to the 1*M* polytype. In particular, the following samples were considered: (1) phlogopite and Fe-rich phlogopite crystals from the alkaline-carbonatite plutonic complex of Tapira, characterized by a crystallization which occurred at a high crustal level, a high cooling rate and an oxygen fugacity above the NNO buffer (Brigatti *et al.*, 1996, 2001); (2) Fe-rich phlogopite crystals from the plutonic complex of Valle del Cervo (Vercelli, Northwestern Italy). Host rocks are granites, syenites and monzonites (Brigatti and Davoli 1990); (3) Fe-rich phlogopite and Mg-rich annite crystals from the mafic enclaves in the Warburton granodiorite. The Warburton complex is a small intrusion, which cooled relatively quickly at a high crustal level (Brigatti *et al.*, 1998).

From a crystal chemical point of view, the factor with the greatest impact on the crystal structure, when considering these samples, is Ti content. In particular, Ti content is strictly related to the distortion in the octahedral sheet. Figure 5 introduces the projection on (001) of the 'octahedral hexagon' defined by the O3 oxygen atoms, with the O4 oxygen atom placed at its 'center'. In Figure 6a,b, Ti content is plotted *vs.* the difference between $(O3-O3)_{M1}$ and $(O3-O3)_{M2}$ distances projected on (001), and *vs.* the *M*1–O4 bond distance projected on (001), respectively. Both illustrations suggest that an increase in Ti content is reflected by an increase in *M*1 site dimensions with respect to *M*2. The explanation of such behavior is straightforward, considering the small dimensions and high charge of the Ti cation, located in *M*2 (Cruciani and Zanazzi, 1994, Cesare *et al.*, 2003, this work). In addition, Figure 6b shows that as Ti content increases, the O4 oxygen atom moves along [100], away from the *M*1 cation and closer to the interlayer cation. As a consequence, the attractive interaction between the O4 oxygen and the interlayer cation increases and the interlayer separation decreases, further confirming the Ti-oxy substitution mechanism.

The displacement of the O4 oxygen atom is also correlated with the distortion of the hexagon and with the increase in the *M*1 site dimension with respect to *M*2. As is apparent from Figures 5 and 6b, the O4 oxygen atom, moving away from *M*1, contributes to the increase

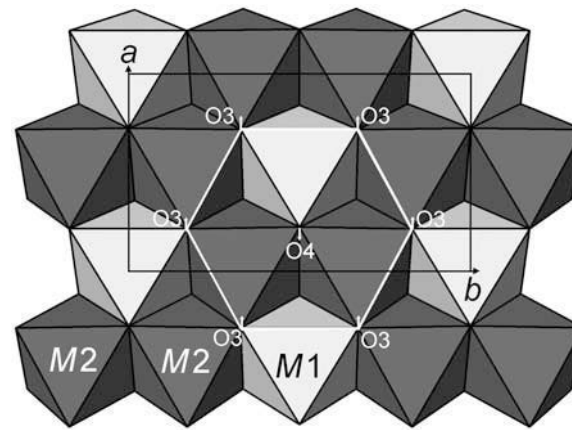

Figure 5. Undistorted octahedral sheet. Note the hexagon ("octahedral hexagon") defined by O3 oxygen atoms (white lines with O4 at its center). Arrows represent two distortion mechanisms along [100] related to Ti content into mica layer: as Ti content increases the O3 oxygen atom displaces along [100] toward *M*2, whereas the O4 oxygen atom displaces along [100] away from *M*1. Unit-cell parameters in black lines.

https://doi.org/10.1346/CCMN.2005.0530208 Published online by Cambridge University Press

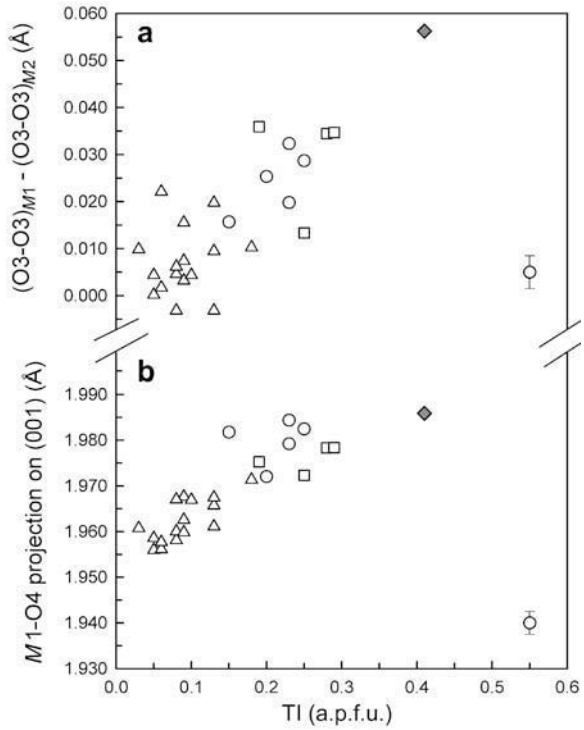

Figure 6. Effect of Ti on 'octahedral hexagon' distortion. (a) Increase of $O3-O3_{M1}$ and concomitant decrease of $O3-O3_{M2}$. (b) Offset of the O4 oxygen atom from the 'octahedral hexagon center' as a function of Ti. Filled diamond: this study; open symbols: samples from the literature (triangles: from Brigatti *et al*., 1996, 2001; circles: from Brigatti and Davoli, 1990; squares: from Brigatti *et al*., 1998), see text.

in the dimension of the *M*1 site. Figure 7, which relates the displacement of the O4 oxygen atom from the 'octahedral hexagon' center and the difference between *M*1 and *M*2 'hexagon edges', further confirms this conclusion. Another mechanism accounting for the increase in the *M*1 site is the translation of the hexagon along [100], towards *M*2, thus in an opposite sense to the displacement of the O4 oxygen atom. This mechanism also was found to be related to Ti content.

CONCLUSIONS

In the present work a chemical and structural characterization of Ti-bearing trioctahedral micas from Black Hill (Australia) was accomplished using a multi-analytical approach. The results can be summarized as follows: (1) Black Hill micas are phlogopite–annite solid-solutions characterized by remarkable compositional homogeneity and a high Ti content (~0.40 a.p.f.u.); (2) SCXRD analysis of polytype 1*M* provided structural evidence for the occurrence of Ti-oxy substitutions; (3) Mössbauer investigation yielded $Fe^{2+}/Fe^{3+} \approx 30$; (4) XPS investigations of Ti speciation provided $Ti^{3+}/Ti^{4+} \approx 0.30$ and suggested the occurrence of a small amount of tetrahedral Ti^{4+}.

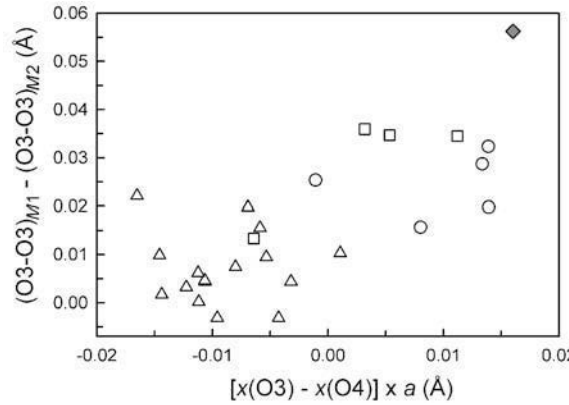

Figure 7. Relationship between the hexagon distortion and the O4 oxygen atom offset. Symbols as in Figure 6.

The substitutions affecting the Black Hill mica structure seem to be as follows: the mechanism $^{XII}K^{+} + {}^{IV}Al^{3+} \rightleftharpoons {}^{XII}\square + {}^{IV}Si^{4+}$ affects 5% of the interlayer cations; the Al-Tschermak substitution, $^{VI}R^{2+} + {}^{IV}Si^{4+} \rightleftharpoons {}^{VI}Al^{3+} + {}^{IV}Al^{3+}$, the Fe-Tschermak substitution, $^{VI}R^{2+} + {}^{IV}Si^{4+} \rightleftharpoons {}^{VI}Fe^{3+} + {}^{IV}Al^{3+}$, the Ti^{4+}-oxy substitution, $^{VI}R^{2+} + 2(OH)^{-} \rightleftharpoons {}^{VI}Ti^{4+} + 2O^{2-} + H_2$, and the Ti^{3+}-oxy substitution affect 5%, 1%, 10% and 3%, respectively, of the octahedral cations. In addition, 1% of tetrahedral cations seem to be involved in the $^{IV}Ti^{4+} \rightleftharpoons {}^{IV}Si^{4+}$ substitution.

Finally, structural distortions related to the Ti content are analyzed and compared to those found in other 1*M* phlogopites of intrusive origin. It was found that, as the Ti increases, oxygens O3 and O4 are displaced in opposite senses along the [100] direction. The resulting distortion accounts for the increase in the size of the *M*1 site with respect to *M*2 and for a decrease in the interlayer separation and is consistent with the occurrence of a Ti-oxy substitution.

ACKNOWLEDGMENTS

Prof. S.P. Turner is acknowledged for providing the mica samples analyzed in the present work. The authors are grateful to Mr Marcello Serracino for assistance during electron microprobe analyses at the Istituto di Geologia Ambientale e Geoingegneria, CNR, Rome. This work was supported by COFIN-MIUR (2002).

REFERENCES

Bohlen, S.R., Peacor, D.R. and Essene, E.J. (1980) Crystal chemistry of a metamorphic biotite and its significance in water barometry. *American Mineralogist*, **65**, 55–62.

Brigatti, M.F. and Davoli, P. (1990) Crystal structure refinement of 1*M* plutonic biotites. *American Mineralogist*, **75**, 305–313.

Brigatti, M.F. and Guggenheim, S. (2002) Mica crystal chemistry and the influence of pressure, temperature and solid solution on atomistic models. Pp. 1–97 in: *Micas: Crystal Chemistry and Metamorphic Petrology* (A. Mottana, F.P. Sassi, J.B. Thompson and S. Guggenheim, editors). Reviews in Mineralogy and Geochemistry, **46**. Mineralogical Society of America and the Geochemical

Society, Washington, D.C.
Brigatti, M.F., Galli, E. and Poppi, L. (1991) Effect of Ti substitution in biotite-1*M* crystal chemistry. *American Mineralogist*, **76**, 1174–1186.
Brigatti, M.F., Medici, L., Saccani, E. and Vaccaro, C. (1996) Crystal chemistry and petrologic significance of Fe^{3+}-rich phlogopite from the Tapira carbonatite complex, Brazil. *American Mineralogist*, **81**, 913–927.
Brigatti, M.F., Lugli, C., Poppi, L. and Elburg, M. (1998) Crystal chemistry of biotites from mafic enclaves in the Warburton granodiorite, Lachlan Fold Belt (Australia). *European Journal of Mineralogy*, **10**, 855–864.
Brigatti, M.F., Medici, L., Poppi, L. and Vaccaro, C. (2001) Crystal chemistry of trioctahedral micas-1*M* from Alto Paranaíba Igneous Province, South-Eastern Brazil. *The Canadian Mineralogist*, **39**, 1333–1345.
Burns, R.G. (1970) *Mineralogical Applications of Crystal Field Theory*. Pp. 53, 59, 124. Cambridge University Press, Cambridge, UK.
Cesare, B., Cruciani, G. and Russo, U. (2003) Hydrogen deficiency in Ti-rich biotite from anatectic metapelites (El Joyazo, SE Spain): Crystal-chemical aspects and implications for high-temperature petrogenesis. *American Mineralogist*, **88**, 583–595.
Cruciani, G. and Zanazzi, P.F. (1994) Cation partitioning and substitution mechanism in 1*M* phlogopite: A crystal chemical study. *American Mineralogist*, **79**, 289–301.
Cruciani, G., Zanazzi, P.F. and Quartieri, S. (1995) Tetrahedral ferric iron in phlogopite, XANES and Mössbauer comparison to single-crystal X-ray data. *European Journal of Mineralogy*, **7**, 255–265.
de Groot, F.M.F., Figueireido, M.O., Basto, M.J., Abbate, M., Petersen, H. and Fuggle, J.C. (1992) 2p X-ray Absorption of Titanium in minerals. *American Mineralogist*, **19**, 140–147.
Desimoni, E. and Malitesta, C. (1986) Interfacing an LHS10 Photoelectron Spectrometer to a microcomputer: Data acquisition and analysis. *Computer Enhanced Spectroscopy*. **3**, 107–112.
Donnay, G., Morimoto, N., Takeda, H. and Donnay, J.D.H. (1964a) Trioctahedral one-layer micas. I. Crystal structure of a synthetic iron mica. *Acta Crystallographica*, **17**, 1369–1373.
Donnay, G., Donnay, J.D.H. and Takeda, H. (1964b) Trioctahedral one-layer micas. II Prediction of the structure from composition and cell dimensions. *Acta Crystallogaphica.*, **17**, 1374–1381.
Ďurovíč, S. (1981) OD-character, Polytypie und identifikation von Schichtsilikaten. *Fortschritte der Mineralogie*, **59**, 191–226.
Ďurovíč, S. (1994) Classification of phyllosilicates according to the symmetry of their octahedral sheets. *Ceramics – Silikàty*, **38**, 81–84.
Dyar, M.D., Guidotti, C.V., Holdaway, M.J. and Colucci, M. (1993) Nonstoichiometric hydrogen contents in common rock-forming hydroxyl silicates. *Geochimica et Cosmochimica Acta*, **57**, 2913–2918.
Dymek, R.F. (1983) Titanium, aluminum and interlayer cation substitutions in biotite from high-grade gneisses, West Greenland. *American Mineralogist*, **68**, 880–899.
Farmer, G.L. and Boettcher, A.L. (1981) Petrologic and crystal chemical significance of some deep-seated phlogopites. *American Mineralogist*, **66**, 1154–1163
Foley, S.F. (1989) Experimental constraints on phlogopite chemistry in lamproites: 1. The effect of water activity and oxygen fugacity. *European Journal of Mineralogy*, **1**, 411–426.
Forbes, W.C. and Flower, M.F.J. (1974) Phase relations of titan-phlogopite, $K_2Mg_4TiAl_2Si_6O_{20}(OH)_4$: a refractory in the upper mantle? *Earth and Planetary Science Letters*, **22**, 60–66.
Güven, N. (1971) The crystal structure of $2M_1$ phengite and $2M_1$ muscovite. *Zeischrift für Kristallographie*, **134**, 196–212.
Hawthorne, F.C., Ungaretti, L. and Oberti, R. (1995) Site populations in minerals: terminology and presentation of results. *The Canadian Mineralogist*, **33**, 907–911.
Hazen, R.M. and Burnham, C.W. (1973) The crystal structure of one layer phlogopite and annite. *American Mineralogist*, **58**, 889–900.
Henry, D.J. and Guidotti, C.V. (2002) Titanium in biotite from metapelitic rocks: Temperature effects, crystal-chemical controls, and petrologic applications. *American Mineralogist*, **87**, 375–382.
Kovalenko, N.I., Kashayev, A.A., Znamenskiy, Y.B. and Zhuravleva, R.M. (1968) Entry of titanium into micas (experimental studies). *Geochemica International*, translated from *Geokhimiya*, **11**, 1348–1357.
Malitesta, C., Losito, I., Scordari, F. and Schingaro, E. (1995) XPS investigation of titanium in melanites from Monte Vulture (Italy). *European Journal of Mineralogy*, **7**, 847–858.
Nazzareni, S., Molin, G., Skogby, H. and Dal Negro, A. (2004) Crystal chemistry of Ti^{3+} - Ti^{4+}-bearing synthetic diopsides. *European Journal of Mineralogy*, **16**, 443–449.
North, A.C.T., Phillips, D.C. and Mathews, F.S. (1968) A semi-empirical method of absorption correction. *Acta Crystallographica*, **A24**, 351–359.
Ohta, T., Takeda, H. and Takéuchi, Y. (1982) Mica polytypism: Similarities in the crystal structures of coexisting 1*M* and $2M_1$ oxybiotite. *American Mineralogist*, **67**, 298–310.
Otten, M.T. and Buseck, P.R. (1987) The oxidation state of Ti in hornblende and biotite determined by Electron Energy-Loss Spectroscopy, with inference regarding the Ti substitution. *Physics and Chemistry of Minerals*, **14**, 45–51.
Rager, H., Geiger, C.A. and Stall, A. (2003) Ti (III) in synthetic pyrope: a single crystal paramagnetic study. *European Journal of Mineralogy*, **15**, 697–699.
Rancourt, D.G. (1994a) Mössbauer Spectroscopy of Minerals I. Inadequacy of Lorentzian-line doublets in fitting spectra arising from Quadrupole Splitting Distributions. *Physics and Chemistry of Minerals*, **21**, 244–249.
Rancourt, D.G. (1994b) Mössbauer Spectroscopy of Minerals II. Problems of resolving cis and trans octahedral Fe^{2+} sites. *Physics and Chemistry of Minerals*, **21**, 250–257.
Rancourt, D.G. and Ping, J.Y. (1991) Voigt-based methods for arbitrary-shape static hyperfine parameter distributions in Mössbauer spectroscopy. *Nuclear Instruments and Methods in Physics Research*, **B58**, 85–97.
Rancourt, D.G., Dang, M.Z. and Lalonde, A.E. (1992) Mössbauer spectroscopy of tetrahedral Fe^{3+} in trioctahedral micas. *American Mineralogist*, **77**, 34–43.
Rancourt, D.G., Ping, J.Y. and Berman, R.G. (1994) Mössbauer spectroscopy of minerals III. Octahedral site. Fe^{2+} quadrupole splitting distributions in the phlogopite–annite series. *Physics and Chemistry of Minerals*, **21**, 258–267.
Renner, B. and Lehmann, G. (1986) Correlation of angular and bond length distortions in TO_4 units in crystals. Z*eitschrift für Kristallographie*, **175**, 43–59.
Rieder, M., Cavazzini, G., D'Yakonov, Y.S., Frank-Kamenetskii, V.A., Gottardi, G., Guggenheim, S., Koval, P.V., Müller, G., Neiva, A.M.R., Radoslovich, E.W., Robert, J.-L., Sassi, F.P., Takeda, H., Weiss, Z. and Wones, D.R. (1998) Nomenclature of micas. *The Canadian Mineralogist*, **36**, 905–912.
Righter, K., Dyar, M.D., Delaney, J.S., Vennemann, T.W., Hervig, R.L. and King, P.L. (2002) Correlations of octahedral cations with OH^-, O^{2-}, Cl^-, and F^- in biotite from volcanic rocks and xenoliths. *American Mineralogist*,

87, 142–153.
Robert, J.L. (1976) Titanium solubility in synthetic phlogopite solid solution. *Chemical Geology*, **17**, 213–227.
Schwarcz, H.P. (1967) The effect of crystal field stabilization on the distribution of transition metals between metamorphic minerals. *Geochimica et Cosmochimica Acta*, **31**, 503–517.
Scordari, F., Schingaro, E. and Pedrazzi, G. (1999) Crystal chemistry of melanites from Mt. Vulture (Southern Italy). *European Journal of Mineralogy*, **11**, 855–869.
Shannon, R.D. (1976) Revised effective ionic radii and systematic studies of interatomic distances in halides and chalcogenides. *Acta Crystallographica*, **A32**, 751–767.
Takeda, H. and Ross, M. (1975) Mica polytypism: dissimilarities in the crystal structures of coexisting 1*M* and $2M_1$ biotite. *American Mineralogist*, **60**, 1030–1040.
Toraya, H. (1981) Distortions of octahedra and octahedral sheets in 1*M* micas and the relation to their stability. *Zeitschrift für Kristallographie*, **157**, 173–190.
Trong On, D. and Bonneviot, L. (1992) Titanium sites in titanium silicalites: an XPS, XANES and EXAFS study. *Journal of Molecular Catalysis*, **74**, 233–246.
Turner, S.P. (1996) Petrogenesis of the late-Delamerian gabbroic complex at Black Hill, South Australia: implications for convective thinning of the lithospheric mantle. *Mineralogy and Petrology*, **56**, 51–89.
Virgo, D. and Popp, R.K. (2000) Hydrogen deficiency in mantle-derived phlogopites. *American Mineralogist*, **85**, 753–759.
Waters, D.J. and Charnley, N.R. (2002) Local equilibrium in polymetamorphic gneiss and the titanium substitution in biotite. *American Mineralogist*, **87**, 383–396.
Watkin, D.J. (1992) CRYSTALS, a programmable program. In *Crystallographic Computing 6 – A Window on Modern Crystallography* (H.D. Flack, L. Parkanyi and K. Simon, editors). Oxford Science Publications, Oxford, UK.
Watkin, D.J. (1994) The control of difficult refinements. *Acta Crystallographica*, **A50**, 411–437.
Waychunas, G.A. (1987) Synchrotron radiation in XANES spectroscopy of Ti in minerals: effects of Ti bonding distances, Ti valence and site geometry on absorption edge structure. *American Mineralogist*, **72**, 89–101.
Weiss, Z., Rieder, M., Chmielovà, M. and Krajiček, J. (1985) Geometry of the octahedral coordination in micas: a review of refined structures. *American Mineralogist*, **70**, 747–757.

(*Received 19 March 2004; revised 9 December 2004; Ms. 893; A.E. Peter J. Heaney*)